

Unraveling the complex dynamics of acoustofluidics

J. Oroscó and J. Friend*

Medically Advanced Devices Laboratory, Center for Medical Devices

Department of Mechanical and Aerospace Engineering University of California San Diego, La Jolla, CA 92093-0411 USA

(Dated: April 5, 2022)

Classical modeling of acoustically-driven flows relies almost exclusively on formal expansions about the assumed small magnitude of resulting streaming flows in relation to driving acoustic particle velocities—a condition referred to as “slow streaming.” The highly nonlinear governing equations are made numerically and analytically tractable with this approach. Unfortunately, the order-of-magnitude separation premise is not generally valid within a modern microacoustofluidics context. Perturbation techniques based on this premise fail to properly extract the dynamics. These theories have nonetheless remained in use in modern analyses, often to the detriment of theoretical consistency and versatility. We describe a novel mathematical formalism for analysis and modeling of these severe systems. The framework provides the user greater generality through articulation and direct exploitation of spatiotemporal scale disparities present between the acoustics and remaining dynamics via multiscale differential operations. This is a leap forward from the classical theories Rayleigh first established nearly one hundred fifty years ago. The method is applied to well-known classical problems of semi-infinite extent defined by particle and streaming velocities possessing similar magnitudes: the “fast streaming” condition. The compressible Navier-Stokes equations are solved in an approximate, successive manner, and acoustic and streaming field equations are obtained. The latter implicitly provides a succinct physical origin for observed layering phenomenon in bulk streaming flows, as discussed in detail in [see co-article]. We analytically obtain closed-form equations that explain fast steady-state bulk streaming. The foregoing results are used to derive a non-constitutive upper bound on the energetic conversion efficiency of the driving acoustics to the resultant maximum streaming flow magnitude. Ample comparison is made to the classic literature and theories to connect this work to past efforts by many authors. Rigorous validation is obtained over a broad survey of experimental findings from the recent literature.

I. INTRODUCTION

“Acoustic streaming” is the designation given to a broad class of remarkably useful flows that result from coupling sound waves to a fluid medium [1]. The complex physical processes underlying these flows are fascinating, leading, with regularity, to counterintuitive behaviors. The practical utility of acoustofluidics has been substantiated across a remarkable diversity of applications, including: biosensing [2, 3], medical diagnostics [4, 5], nozzle-free printing [6], smart materials [7], gene editing [8], energy storage [9, 10], drug delivery [11, 12], noise insulation [13], and a great many others [1, 14–17]. This utility underscores the importance of deducing consistent theoretical explanations of acoustofluidic phenomena.

A. On the analysis of acoustic streaming

At the highest level, the difficulty associated with the analysis of acoustofluidic systems can be ascribed to the user’s need to extract the net streaming motions from the flow field as independent from the originating acoustics, all within the mathematical context of the nonlinear governing equations. These are, of course, the celebrated Navier-Stokes equations taken over a compressible medium.

Historically, acoustofluidics modeling of streaming behaviors has been founded, strongly and almost exclusively, upon formal asymptotic expansions in a pertinent small parameter (*e.g.*, the acoustic Mach number) in order to decompose the flow field into its constituent elements. In this approach, streaming flows are regarded as steady “second order quantities” with characteristic flow magnitudes much smaller than the maximum on-source particle velocity. This is referred to as the “slow streaming” approximation. This particular method of decomposing the flow field was first employed by Rayleigh during his study of ordered cells of recirculating flow that develop in Kundt’s tubes [18]. Since then, a number of Rayleigh’s contemporaries—including, among others, Eckart [19], Nyborg [20], and Westervelt [21]—have leveraged this approach in their analyses in order to render the highly nonlinear governing equations tractable.

The tenuous classical conceptions of streaming flows are unsound within the domain of modern acoustofluidics research. Systems in this domain are often characterized by large acoustic intensities and sub-millimeter acoustic wavelengths [12, 22]. In these systems, no baseline assumption about the relative magnitudes of the acoustic and streaming fields can be generally relied upon [23–25], so that formal asymptotic expansions based on the slow streaming assumption are not generally valid [22, 26]. Furthermore, streaming flow is not impulsively generated as a steady quantity. Instead, it is transient, developing over a finite time interval from the application of even a constant acoustic field [27, 28]. And yet the transience of

* Corresponding author: jfriend@ucsd.edu

acoustic streaming is necessarily eliminated by the time average constraints of classical methods [29, 30]. In other words, these traditional approaches often mask, rather than reveal, the physical provenance of streaming flows.

Lighthill addressed this matter in his seminal study on acoustic streaming [31]. He noted that “... the question of whether a term can be neglected or not depends... exclusively on its numerical magnitude and not on its mathematical order,” referring to the slow streaming approximation as “RNW streaming” (after Rayleigh, Nyborg, and Westervelt). And although he proffered a semi-empirical derivation for “fast” bulk jet streaming, he left the more general problem of devising a systematic fast streaming framework unresolved.

Somewhat earlier than Lighthill’s exposition, and on a different continent, the concept of and terminology for fast acoustic streaming was established by Zarembo [32]. He identified the weakness of the asymptotic approach when dealing with large-amplitude acoustic streaming, stating, “The method of successive approximations... is inapplicable in this case.” Zarembo defined flow partitions without any order of magnitude assumption. He instead employed time averaging and an *a priori* density assumption (equivalent to assuming a small acoustic Mach number) to decouple the streaming and acoustic fields. Zarembo concluded his investigation without providing a method for solving the general set of decoupled equations.

Notwithstanding these shortcomings, the classical approach pervades the literature due to a lack of suitable alternatives [30, 33, 34]. In Ref. [30], for example, Vanneste and Bühler study a standard three-phase contact configuration and the physical progression from leaky surface acoustic waves to steady interior streaming. In doing so, they have defined the Eulerian mean field as the second order component in a formal asymptotic expansion about the small acoustic Mach number. The assumption of convergence must later be abandoned to permit inclusion of interior streaming amplitudes that scale with a potentially unbounded characteristic length [35].

The severity of these predicaments is compounded by the ubiquitous presence of enormous disparities between the spatiotemporal scales of the acoustic forcing and those associated with the streaming flow it generates. Scale disparities of between five and nine orders of magnitude are typical [12, 24] and prevent comprehensive characterization, whether by theory or empiricism. For example, in configurations with the most acute scale disparities, full scale numerical simulations that respect a requisite Nyquist mesh across space and time, while also computing over sufficiently large domains for resolving the streaming motions, will consume years of computation time before resolving a single period of fundamental motion. A simple, back-of-the-envelope calculation reveals this to be the case even if the most cutting-edge (at time of writing) technologies are employed: the lattice Boltzmann method with GPU-accelerated parallelization supported by several top-of-the-line graphics cards [36].

And while this modern technological nexus is “infinitely scalable,” modern budgets are not. Likewise, in the laboratory setting, fully resolving the most elusive flow structures at the smallest, fastest scales remains an impossibility with currently available techniques and equipment. For the limited number of microacoustofluidic flows that *can* be empirically characterized, one does so only on availability of the most advanced (and most costly) instrumentation, and often only after extending the novelty of some existing experimental methodology in a nontrivial way.

These challenges are not unique to the study of acoustofluidic systems. They may arise in any nonlinear continuous medium under the influence of high-frequency periodic forcing (including noise forcing). Here our notions of “high” and “low,” “fast” and “slow,” and “large” and “small” are qualified (and further on, more concretely quantified) in terms of the aforementioned scale disparities. Systems that fit these criteria frequently arise in the study of: lasers and laser optics [37, 38], transport in porous media [39], hydrogeologic modeling [40], electrochemistry [41], structural mechanics [42], climate dynamics [43], and rheology [44, 45], to name a few.

Fortunately, however, a glint of opportunity is found in the efforts of some authors [27, 29, 46]. In Ref. [29], Riley couples the imprecision of his analysis to the inverse of a very large Strouhal number. Its largeness is representative of the time scale disparity between the driving acoustics and the ensuing streaming flow. As this disparity grows, the successive approximations are made increasingly accurate. In Refs. [46] and [27], a time scale separation is observed in the differential operations—qualitatively at first in the former and more rigorously in the latter, more recent study. In Ref. [27], formalization of the partitioned time derivative mirrors that of a rigid-body analysis technique that can be said to have originated in the mid-twentieth century [47]. In both studies, streaming transience survives temporal averaging over the acoustic period.

B. Generalized analysis of nonlinear PDEs with acute scale disparities

In the present study, we describe a generalized framework within which an appropriate model of streaming flow from the compressible Navier-Stokes equations may be derived. The framework, denoted the Multiscale Articulated Differentials Method (MADaM), is based upon the need for direct, explicit consideration and exploitation of all spatiotemporal scale disparities—not only with respect to the field variables, but also with respect to the differential operations that compose the governing nonlinear PDEs. A template for this endeavor is found in the aforementioned works of Blekhman [47], and the later works of Thomsen [48]. They delineate a systematic framework (that Blekhman referred to as “vibrational mechanics”) for the analysis of nonlinear rigid-body sys-

tems (*i.e.*, Newtonian systems described by nonlinear ODEs) driven by high-frequency excitation. At the heart of this framework is the Method of Direct Partition (or Separation) of Motions (MDPM). The method exploits temporal scale disparities in order to decompose the nonlinear equations into “fast motions” and “slow motions,” where dynamics in the latter category represent the resultant behaviors of interest. This methodology is notable for its ability to unveil the enigmatic mechanisms underlying the counterintuitive behaviors that one frequently observes in these systems [49].

Previous investigations involving the application of an MDPM-type analysis to continuous systems have focused on temporal partitioning [27, 46, 50]. Here we describe a complete extension of the MDPM into the realm of continuous media, with attention given to scale disparities in both time and space—and their interdependence—during construction of the dynamical partitions. The approach is highly generalized and leads to tractable streaming equations that, by construction, respect the relative magnitudes of the streaming flow and particle velocity.

C. Outline

The remainder of this work proceeds as follows. In Sec. II, we outline the theory surrounding the methodology, beginning with a description of the theoretical foundations of MDPM, proceeding to define the underlying theory of MADaM, and then describing its application to microacoustofluidics within the backdrop of a previously established fast streaming system. In Sec. III, we apply the framework to the well-known quartz wind problem in a one-dimensional context. A nonlinear PDE governing the streaming dynamics is extracted and used to derive an analytical expression to describe the steady flow. Insight into the nature of the streaming flow is gleaned from each expression, eventually producing a fundamental limit governing the conversion efficiency from the source’s particle velocity to the maximum output acoustic streaming velocity. Section IV provides a results-driven analysis of the empirical agreement between the theory and a number of experimental studies from the literature. We conclude in Sec. V with a brief summarizing discussion of the main results.

II. THEORY

A. Notation

In this work, we use a compact form of Leibniz’ notation that combines elements of notation found elsewhere in the literature into a single, consistent framework that maintains the flexibility of the expanded form. To illustrate, we consider the vector-valued function $h_i(x, t)$ of a Euclidean spatial input $x = (x_i, x_j, x_k)$ and the scalar temporal input t , where the vectorial output is given in

indicial notation. We write the substantial derivative of this function as

$$D_t h_j(x, t) = \partial_t h_j(x, t) + u_i(x, t) d_{x,i} h_j(x, t), \quad (1)$$

where the dot product of velocity with the gradient in the last term is represented through the Einstein summation convention.

The use of d represents a derivative that is intradimensionally complete, but interdimensionally partial. The partial operator ∂ is reserved for derivatives that are intradimensionally partial. This is done since it is necessary to differentiate in multiple temporal and spatial scales. For example, we demonstrate further on that it is necessary to expand the time derivative as

$$d_t = \partial_t + \partial_t \tau \partial_\tau, \quad (2)$$

which allows one to differentiate a function of two distinct time scales: t and τ . Wherever convenient, an entire vector, rather than its component, is represented by dropping the index notation, as with the input to Eq. (1). Wherever implicit or contextually understood, we will also drop arguments to functions.

B. MDPM for rigid bodies

The method of direct partition of motions is based on the “[fundamental] assumption of vibrational mechanics” [47]. This assumption is developed around Newtonian systems of the form

$$m \ddot{x} = F(\dot{x}, x, t) + \Phi(\dot{x}, x, t, \tau), \quad (3)$$

where $(\dot{x}, \ddot{x}) = (d_t x, d_t^2 x)$ and where relevant components may be vectorial as dictated by the application. Here Φ represents forces of approximate temporal periodicity that are a function of a “fast” time scale $\tau = \omega t$, with $\omega \gg 1$ being a large parameter. The forces F are therefore “slow,” being a function only of the slow time scale t . Our notions of fast and slow are made explicit in the [supplemental information].

The fundamental assumption of vibrational mechanics (FAVM) is that the system given in Eq. (3) has time scale-partitioned solutions that, in Blekhman’s notation, have the form

$$x(t, \tau) = \Psi(t, \tau) + X(t), \quad (4)$$

which we refer to as the fundamental equation of vibrational mechanics (FEVM). Equation (4) may also be vectorial as dictated by Eq. (3). Here X represents slow behaviors and Ψ represents fast behaviors, the latter typically being strongly correlated with the high-frequency forcing. This last assumption of correlation can often be validated by direct empirical measurement of the system under study [12].

The underlying idea in this approach is that the observed slow motions are assumed to be an average result

of the system dynamics. The dynamics act as a nonlinear filter for the input forces. By formalizing the timescales in terms of the characteristic scales— X_0 and Ψ_0 for the slow and fast motions, respectively—one can show that

$$\frac{d_t^n X}{d_t^n \Psi} \sim \varepsilon^{n-k}. \quad (5)$$

where $\varepsilon = \omega^{-1} \ll 1$, and with $k \in \mathbb{Z}$ as determined by the relation

$$\frac{\Psi_0}{X_0} \sim \varepsilon^k. \quad (6)$$

With $n \in \mathbb{Z} \geq 0$, we can use Eq. (6) to generate differential scaling associations such as

$$k = 1 : X/\Psi \sim 1/\varepsilon, \quad \dot{X}/\dot{\Psi} \sim 1, \quad \ddot{X}/\ddot{\Psi} \sim \varepsilon, \quad (7a)$$

$$k = 2 : X/\Psi \sim 1/\varepsilon^2, \quad \dot{X}/\dot{\Psi} \sim 1/\varepsilon, \quad \ddot{X}/\ddot{\Psi} \sim 1. \quad (7b)$$

We will refer to Eq. (7a) as the “traditional” MDPM, since it leads to the nondimensional positional FEVM

$$x_* = X_* + \varepsilon \Psi_*, \quad (8)$$

and this is the form most commonly encountered in the literature. After substituting the partitioned variables and operators into the nondimensionalized equation of motion, and then applying the differential (instantaneous change rate) and integral (averaging) constraints, one arrives at a finite-term equation written in terms of the small parameters. This equation is physically derived, rather than defined. It nonetheless permits an analytical approach that is analogous to perturbation expansion.

1. Example: Pendulum affixed to a vibrating support

The utility of the MDPM is best illustrated with a simple example: a rigid-body pendulum attached to a rapidly vibrating support. We provide here a brief sketch of the more elaborate investigation described by Thomsen starting on p. 292 of Ref. [49]. In Thomsen’s notation, the nondimensional equation of motion is written

$$\ddot{\theta} + 2\beta\dot{\theta} + (1 - q\Omega^2 \sin \Omega t) \sin \theta = 0, \quad (9)$$

where θ is the angular position, β is the damping ratio, $q \ll 1$ is a nondimensional support oscillation amplitude, and $\Omega \sim q^{-1} \gg 1$ is the nondimensional forcing frequency.

One begins by defining a “fast” time scale $\tau = \Omega t$, and fast and slow positional variables, $\varphi(t, \tau)$ and $z(t)$, respectively. Then the nondimensional FEVM is $\theta(t, \tau) = z(t) + \Omega^{-1}\varphi(t, \tau)$, which corresponds to Eq. (8). We will show further on how this is analogous to large-amplitude streaming. For now, it is sufficient to note Eq. (7a), which rigorously establishes that the ratio of velocities must be $\dot{z}/\dot{\varphi} = \mathcal{O}(1)$.

Thomsen applied the foregoing framework to show that the fast motions can be written

$$\varphi(t, \tau) = -q\Omega \sin z \sin \tau + \mathcal{O}(\Omega^{-1}), \quad (10)$$

and also that the slow motions can be approximated with

$$\ddot{z} + 2\beta\dot{z} = \mathcal{T}_r(z) + \mathcal{O}(\Omega^{-1}), \quad (11)$$

where

$$\mathcal{T}_r(z) = -\left(1 + \frac{1}{2}(q\Omega)^2 \cos z\right) \sin z \quad (12)$$

is a position-dependent restoring torque. Equation (11) has been decoupled from the fast motion variable and may therefore be solved numerically with an enormous reduction in computational expense.

If we now consider the rotational stiffness, $k_r = -d\mathcal{T}_r/dz$, at the equilibrium points

$$k_r = \begin{cases} \frac{1}{2}(q\Omega)^2 + 1 & \text{if } z = 0 \\ \frac{1}{2}(q\Omega)^2 - 1 & \text{if } z = \pm\pi \end{cases}, \quad (13)$$

we find the origin of an empirically observed, counterintuitive physical phenomenon. In particular, when $(q\Omega)^2 < 2$, the downward hanging position ($z = 0$) is stable and the upward position ($z = \pm\pi$) is unstable. That is, if moved away from these positions, the system will depart from or return to the position, respectively. However, when $(q\Omega)^2 > 2$, the rotational stiffness at the upright position ($z = \pm\pi$) changes sign and the upright position becomes a stable equilibrium position. Attempts to push it out of this equilibrium position are met by an opposing torque proportional to the rotational stiffness value $\frac{1}{2}(q\Omega)^2 - 1 > 0$.

C. MADaM: An acoustofluidic extension

In order to properly extend the tenets of MDPM to the acoustofluidic setting, it is necessary to understand, from fundamental principles, how one arrives at the dimensionless expressions traditionally encountered in the literature when applying the MDPM to ordinary differential relations [47–49, 51]. We begin with the convention of assuming that the flow is superposed of, or “partitioned” into the “slow” (streaming) and “fast” (acoustic) components:

$$\tilde{u}_i(\tilde{x}, \tilde{t}) = \tilde{u}_i^{(s)}(\tilde{x}, \tilde{t}) + \tilde{u}_i^{(a)}(\tilde{x}, \tilde{t}), \quad (14)$$

where we have used index notation and where we denote all dimensional field variables, operators, and independent parameters with a tilde.

1. Fast streaming axiom

For context, we take as our template system the surface acoustic wave (SAW)-driven laminar jet streaming

described in Refs. [24, 52], which represents an extension of Lighthill’s well-known turbulent jet model [31] for use in microacoustofluidic systems. In Refs. [24, 52], the maximum streaming jet velocity, U_s , may generally be of the same order of magnitude as the on-source particle velocity, U_a .

If we define the characteristic jet streaming length as x_s and the corresponding streaming time scale as $t_s = x_s/U_s$, then we are free to write:

$$\tilde{u}_i = \frac{x_s}{t_s} u_i^{(s)} + \xi_p \omega u_i^{(a)}, \quad (15)$$

where the particle displacement is ξ_p , and the acoustic time scale, $1/\omega$, is given in terms of the angular acoustic frequency $\omega = 2\pi f$. The absence of a tilde indicates nondimensional field variables, operators, and independent parameters. The nondimensionalized velocity is thus written

$$u_i(x, \xi, t, \tau) = u_i^{(s)}(x, t) + q_p S u_i^{(a)}(x, \xi, t, \tau), \quad (16)$$

with $q_p = \xi_p/x_s \ll 1$ and $S = \omega t_s \gg 1$, and where the nondimensional time variables t and τ , and the nondimensional space variables x_i and ξ_i , are defined further on. For now it is sufficient to note that t and x refer to large streaming scales, while τ and ξ refer to small acoustic scales. Clearly then, the assumption made in Eq. (16) is that the nondimensional streaming velocity changes only over large space scales and over long times relative to the small acoustic scales and short wave periods—an assumption that is valid within the present context.

Since, by our earlier definition, the streaming and particle velocity magnitudes are of the same order, Eq. (15) tells us that

$$\frac{x_s}{\xi_p} \sim \omega t_s, \quad (17)$$

so that $q_p S \sim 1$. Within the present framework, this simple-yet-fundamental result may be regarded as a fast streaming axiom (FSA) upon which the remainder of the scales are developed.

2. Temporal derivative partitioning

We formalize the time scale separation by deriving a time differential that is intradimensionally complete and interdimensionally partial. Let the dimensional form of this operator be \tilde{d}_t and hence denote the flow unsteadiness

$$\tilde{d}_t \tilde{u}_i = \tilde{d}_t \tilde{u}_i^{(s)} + \tilde{d}_t \tilde{u}_i^{(a)}. \quad (18)$$

This expression makes it clear that a single scale is insufficient for properly nondimensionalizing the time differential: the flow components possess drastically different characteristic change rates. We therefore define two

nondimensional time scales, both originating from “real” (*i.e.*, physical) time:

$$t = \frac{1}{t_s} \tilde{t}, \quad (19a)$$

$$\tau = \omega \tilde{t}, \quad (19b)$$

and observe that $t_s t = \tilde{t} = \frac{1}{\omega} \tau$, with, in particular, $\tau = S t$, so that for any small change in the “slow” time scale δt there is a corresponding large change in the “fast” time scale $\delta \tau = S \delta t$, which yields, in the limit, $d\tau/dt = S$.

For any nondimensional field variable $\chi(t, \tau)$ that is a function of both timescales, differentiating with respect to time in the nondimensional space requires the total differential

$$\begin{aligned} \tilde{d}_t &= \tilde{\partial}_t \partial_t + \tilde{\partial}_t \tau \partial_\tau \\ &= \frac{1}{t_s} \partial_t + \omega \partial_\tau, \end{aligned} \quad (20)$$

so that the nondimensional total temporal differential is

$$d_t = S^{-1} \partial_t + \partial_\tau. \quad (21)$$

3. Spatial derivative partitioning

The need to partition and scale differential operations subtends not only temporal differentiation, but also—by directly analogous reasoning—spatial differentiation. Proceeding as in the temporal case, we denote our gradient operator in index notation as $\tilde{d}_{x,i}$, so that, under the traditional flow partition Eq. (14), the velocity gradient is

$$\tilde{d}_{x,i} \tilde{u}_j(\tilde{x}, \tilde{t}) = \tilde{d}_{x,i} \tilde{u}_j^{(s)}(\tilde{x}, \tilde{t}) + \tilde{d}_{x,i} \tilde{u}_j^{(a)}(\tilde{x}, \tilde{t}), \quad (22)$$

The characteristic distance over which the acoustic component varies is, of course, the spatial wave period $\lambda = 2\pi/k$, with k being the acoustic wavenumber. Then the need (or lack thereof) to partition the gradient operator in any given coordinate direction will depend on the disparity (or lack thereof) between the wavelength and the streaming space scale in that particular coordinate. For our contextual bulk jet streaming example (and indeed, in most bulk streaming scenarios), we have $x_s \gg \lambda$.

Strictly speaking, one could consider a unique spatial partitioning along each coordinate direction, invoking a Hadamard product in the derivative definition to follow. However, in order to more simply delineate the theory, we assume a single partition (*i.e.*, a single spatial scale disparity parameter), which is appropriate for the one-dimensional example provided further on. We define two nondimensional spatial scales

$$x_i = \frac{1}{x_s} \tilde{x}_i, \quad (23a)$$

$$\xi_i = k \tilde{x}_i, \quad (23b)$$

which lead to the nondimensional total spatial gradient

$$d_{x,i} = q_\lambda \partial_{x,i} + \partial_{\xi,i}, \quad (24)$$

where $q_\lambda = (k x_s)^{-1} \ll 1$ characterizes the spatial scale disparity for our present case.

4. Velocity partition

We complete our analysis by decomposing a positional description—a trajectory—for the fluid parcel:

$$\begin{aligned} \tilde{r}_i(\tilde{x}, \tilde{t}) &= \tilde{r}_i^{(s)}(\tilde{x}, \tilde{t}) + \tilde{r}_i^{(a)}(\tilde{x}, \tilde{t}), \\ &= x_s r_i^{(s)}(x, t) + \xi_p r_i^{(a)}(x, \xi, t, \tau), \end{aligned} \quad (25)$$

and express its nondimensional counterpart

$$r_i = r_i^{(s)} + q_p r_i^{(a)}, \quad (26)$$

which corresponds to the traditional MDPM scaling category of Eq. (7a).

To see how our MDPM trajectory expression relates to the nondimensionalization in Eq. (16), we must recall that the trajectory is related to the velocity within a Navier-Stokes formulation. Note that the Lagrangian and Eulerian velocities are given in terms of the time derivative of the trajectory, and they are made equivalent by requiring that they be applied along a particular fluid parcel trajectory. Then

$$u_i = d_t r_i \approx \partial_t r_i^{(s)} + q_p \partial_t r_i^{(a)} + q_p S \partial_\tau r_i^{(a)}. \quad (27)$$

With the intuitive definitions (guided by the associated characteristic scales) $u_i^{(s)} = \partial_t r_i^{(s)}$ and $u_i^{(a)} = \partial_\tau r_i^{(a)}$, along with the auxiliary “modulated particle velocity” definition $u_i^{(m)} = \partial_t r_i^{(a)}$, we arrive at

$$u_i \approx u_i^{(s)} + q_p S u_i^{(a)} + q_p u_i^{(m)}, \quad (28)$$

where the first two terms on the right-hand side are $\mathcal{O}(1)$ and the last term on the right-hand side is $\mathcal{O}(\varepsilon)$. This suggests the dimensional form $\tilde{u}_i = \tilde{u}_i^{(s)} + \tilde{u}_i^{(a)} + \tilde{u}_i^{(m)}$, with $\tilde{u}_i^{(m)}$ having the mixed-scale characteristic value ξ_p/t_s . When originated from a positional description, our analysis yields a velocity partition with an additional term bearing $\mathcal{O}(\varepsilon)$ importance. This term may be interpreted as a potentially necessary correction due to a particle velocity waveform with an amplitude that is modulated over time scales that are much larger than an acoustic period. This modulation could, for example, be applied during experimentation. When no such modulation occurs, as will henceforth be assumed, this term vanishes.

Comparing Eq. (28) with Eq. (16)—the latter being essentially a nondimensionalization of Zaremba’s method for “fast streaming” [32]—we see that the auxiliary term

represents a perturbative correction to the classical approach. We recall that Zaremba’s method avoids expansion about the smallness of the streaming velocity since, by definition, no such order of magnitude separation exists in fast streaming systems. The difference in Eq. (28) is that the smallness of $q_p \sim S^{-1}$ is ensured since $S \gg 1$ due to the enormous time scale separation between the fast and slow dynamics.

5. Physical constraints in the nondimensional space

As in the case of traditional MDPM applied to rigid body ODEs, the application of MADaM necessitates the usage of additional physical constraints for closure in light of additional unknown variables. These constraints are applied to either average (integral) or instantaneous (differential) behaviors. We employ the intermediate nondimensional value τ_∞ such that $1/\omega \ll \tau_\infty \ll t_s$ with the separation being great enough that we may take τ_∞ to be the stationary limit of the acoustic field while leaving the transience of the streaming field intact.

We define the stationary acoustic (“fast time”) temporal average

$$\begin{aligned} \langle (\cdot) \rangle_\tau &= \frac{\omega}{2\pi} \int_0^{2\pi/\omega} \lim_{\tilde{t} \uparrow \tau_\infty/\omega} (\cdot) d\tilde{t} \\ &= \frac{1}{2\pi} \int_0^{2\pi} \lim_{\tau \uparrow \tau_\infty} (\cdot) d\tau, \end{aligned} \quad (29)$$

and the acoustic spatial average—a unity-weighted convolution that retains the x-coordinate dependence:

$$\langle (\cdot) \rangle_\xi = \left(\frac{1}{2\pi} \right)^3 \iiint_{\xi-\pi}^{\xi+\pi} (\cdot) d\xi_{i,j,k}^t, \quad (30)$$

taken over a small containing cube with edge length $\lambda = 2\pi/k$. Our differential and integral constraints are accordingly written

$$\partial_\tau u_i \approx q_p S \partial_\tau u_i^{(a)}, \quad (31a)$$

$$\langle u_i \rangle_\tau \approx u_i^{(s)}, \quad (31b)$$

$$\partial_{\xi,i} u_j \approx q_p S \partial_{\xi,i} u_j^{(a)}, \quad (31c)$$

$$\langle u_i \rangle_\xi \approx u_i^{(s)}. \quad (31d)$$

There remains a question of the validity of Eq. (31d), or more explicitly, a question of whether it is reasonable to assume that $\langle u_i^{(a)} \rangle_\xi \approx 0$. While this issue should be taken up on a case-by-case basis, we contend that for many useful systems it can be expected to hold to sufficient approximation.

For example, consider our contextual scenario of laminar jet streaming [24]. We can model an attenuating acoustic plane wave propagating into the fluid medium along a Poynting vector aligned with the jet axis \tilde{x}_i as

$$\tilde{u}^{(a)}(\tilde{x}, \tilde{t}) = U_a \exp[\iota(\kappa \tilde{x}_i - \omega \tilde{t})], \quad (32)$$

where $\iota = \sqrt{-1}$ and the complex wavenumber is $\kappa = k + \iota\alpha$, given in terms of the attenuation coefficient $\alpha = \delta_a^{-1}$, with δ_a being the attenuation length. In using complex exponentials, it is assumed throughout that only the real value is recovered. We recall that the source particle velocity $U_a = \xi_p \omega$. The magnitude of the effect of the asymmetries will depend on the extent of the attenuation over a given spatial period [see supplementary materials, Fig. 1], so that the ratio of interest is $\kappa_i = (k \delta_a)^{-1}$. As $\kappa_i \rightarrow 0$, the wave is negligibly attenuated over a single spatial period, so that antisymmetry remains intact and the spatial average returns zero. We write the nondimensionalized spatial average taken in the direction of propagation as

$$\begin{aligned} \max_{\tilde{x}_i \geq \pi/k} |\langle u_i^{(a)} \rangle_{\xi, i}| &= \max_{\tilde{x}_i \geq \pi/k} \left| \frac{k}{2\pi} \int_{\tilde{x}_i - \pi/k}^{\tilde{x}_i + \pi/k} \frac{\tilde{u}^{(a)}}{U_a} d\tilde{x}_i \right| \\ &= \frac{1}{\pi} \psi_0(\xi_{0, \max}) \sinh \pi \kappa_i \\ &\approx \theta \end{aligned} \quad (33)$$

where the approximation is valid, $\psi_0(\xi_{0, \max}) \approx 1$, and $\kappa_i \approx \theta \equiv \mu_l \omega / 2 \rho_0 c^2$ when $\kappa_i \ll 1$. Guided by the Navier-Stokes equations, we also consider averages of up to second-order gradient fields:

$$\max_{\tilde{x}_i \geq \pi/k} |\langle d_{\xi, i} u_i^{(a)} \rangle_{\xi, i}| = \frac{1}{\pi} \psi_1(\xi_{1, \max}) \sinh \pi \kappa_i \approx \theta, \quad (34a)$$

$$\max_{\tilde{x}_i \geq \pi/k} |\langle d_{\xi, i}^2 u_i^{(a)} \rangle_{\xi, i}| = \frac{1}{\pi} \psi_2(\xi_{2, \max}) \sinh \pi \kappa_i \approx \theta, \quad (34b)$$

which have been normalized by $U_a k$ and $U_a k^2$, respectively. When $\kappa_i \gtrsim 1$, we must use the full expressions

$$\psi_0(\xi) = \frac{e^{-\kappa_i \xi} (\kappa_i \cos \xi - \sin \xi)}{\kappa_i^2 + 1}, \quad (35a)$$

$$\psi_1(\xi) = -e^{-\kappa_i \xi} \cos \xi, \quad (35b)$$

$$\psi_2(\xi) = -e^{-\kappa_i \xi} (\kappa_i \cos \xi + \sin \xi), \quad (35c)$$

with $\xi_{0, \max} = 3\pi/2$, $\xi_{1, \max} = \arccos(-1/\sqrt{\kappa_i^2 + 1})$, and $\xi_{2, \max} = \pi + \arccos(2\kappa_i/\sqrt{\kappa_i^2 + 1})$.

Using the foregoing results, we can now place bounds on the validity of spatial averaging. For $\kappa_i \lesssim 0.15$, all noted normalized spatial averages return an absolute maximum residual $\lesssim 0.1$. Since Eq. (32) is a function only of the \tilde{x}_i coordinate, averaging across the remaining dimensions leaves this result unchanged. This establishes a rule of thumb that Eq. (31d) is valid, and also that $\langle d_{\xi, i} u_i^{(a)} \rangle_{\xi} \approx 0$ and $\langle d_{\xi, i}^2 u_i^{(a)} \rangle_{\xi} \approx 0$, so long as $\lambda \lesssim \delta_a$, a condition that is satisfied by an acoustofluidic system operating at less than roughly 25 GHz (for water), as shown in Fig. 1.

Virtually all acoustofluidics phenomena to date occur at < 2 GHz, well within the conditional range of our analysis. Indeed, from an order of magnitude perspective, the valid range of the analysis exhausts the domain of continuum mechanics. We identify the valid range of

continuum mechanics for acoustofluidics with an upper bound at $Kn \sim 0.01$, where we define the Knudsen number, $Kn = \ell/\delta_a$, in terms of the mean free path ℓ . We have used the attenuation length as a characteristic scale rather than using wavelength. The limit defined in terms of the former is $f \sim 40$ GHz, whereas the limit defined in terms of the latter is $f \sim 60$ GHz.

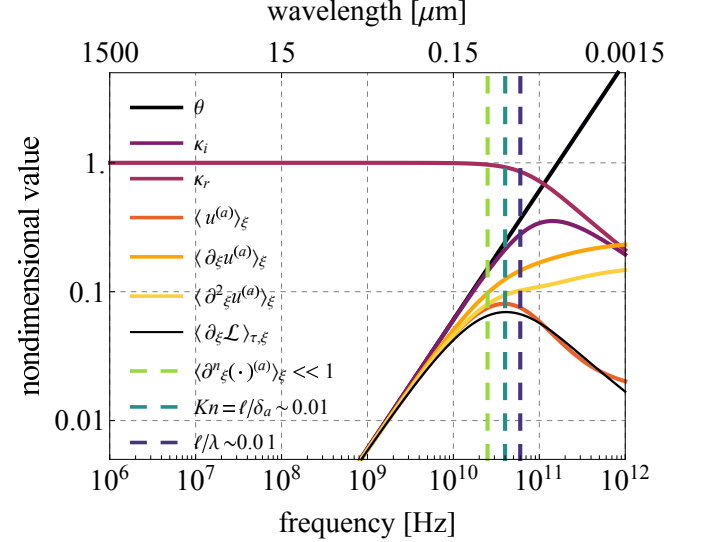


FIG. 1. Important frequency-dependent nondimensional values for water (some of which are defined further on). The $\lambda \lesssim \delta_a$ limit corresponds to an upper bound on frequency of roughly 25 GHz (vertical, dashed, light green). Trends below this limit continue to lower frequencies unabated. Averages of the acoustic wave remain approximately valid throughout the applicable domain of continuum mechanics. The upper bound of roughly 40 GHz for this domain is determined by the Knudsen number $Kn \sim 0.01$ (vertical, dashed, green), defined as the ratio of the mean free path ($\ell \approx 270$ pm) of the individual water molecules to the acoustic wave attenuation length. When $Kn \gtrsim 0.01$, a phonon-based recasting of the representative equations may prove useful.

III. ONE-DIMENSIONAL BULK STREAMING

Having sufficiently developed the underpinning theory for the MADaM, we now set upon its application to an example system. We consider an acoustic wave traveling into an unbounded water medium and manipulate the distal streaming field boundary in order to demonstrate how the more general result underlies bulk streaming in differing configurations.

The isentropic, compressible Navier-Stokes equations in one Cartesian dimension are

$$\tilde{\rho} \tilde{D}_t \tilde{u}_x = -\tilde{d}_x \tilde{P} + \mu_l \tilde{d}_x^2 \tilde{u}_x + \tilde{F}_x, \quad (36a)$$

$$\tilde{d}_t \tilde{u}_x + \tilde{d}_x (\tilde{\rho} \tilde{u}_x) = 0, \quad (36b)$$

$$\tilde{P} = \tilde{P}(\tilde{\rho}), \quad (36c)$$

with longitudinal viscosity $\mu_l = \mu_s(4/3 + \mu_v/\mu_s)$ written in terms of the shear viscosity, μ_s , and the volume viscosity, μ_v . Expanding the equation of state about its nominal hydrostatic condition leads to

$$\frac{\tilde{P}'}{A} = s + \frac{B}{2A}s^2 + \mathcal{O}(s^3), \quad (37)$$

where $\tilde{P}' = \tilde{P} - P_0$ and the condensation, $s = \tilde{\rho}'/\rho_0$, is given in terms of the density variations $\tilde{\rho}' = \tilde{\rho} - \rho_0$. The quantity B/A is Beyer's parameter characterizing the nonlinearity of the system [53]. If the medium under consideration is water and the conditions are fast streaming—as in Refs. [23, 24, 52]—then the first term is $\mathcal{O}(10^{-4})$ and the second term is $\mathcal{O}(10^{-8})$. We conduct the present analysis within the context of the previously discussed laminar jet streaming system.

Following Riley [29], we differentiate Eq. (36a) with respect to time, substitute both Eq. (36b) and the linear expansion of Eq. (36c) into the result, and arrive at

$$\begin{aligned} & \tilde{\rho} \tilde{d}_t \tilde{D}_t \tilde{u}_x - \tilde{d}_x(\tilde{\rho} \tilde{u}_x) \tilde{D}_t \tilde{u}_x \\ & = c^2 \tilde{d}_x^2(\tilde{\rho} \tilde{u}_x) + \mu_l \tilde{d}_x^2 \tilde{d}_t \tilde{u}_x + \tilde{d}_t \tilde{F}_x. \end{aligned} \quad (38)$$

A. Density partition

In order to proceed within the principles of the established framework, we must first define a physically and theoretically consistent density partition:

$$\tilde{\rho}(x, \xi, t, \tau) - \rho_0 = \tilde{\rho}^{(s)}(x, t) + \tilde{\rho}^{(a)}(x, \xi, t, \tau), \quad (39)$$

where ρ_0 is the unperturbed fluid density, and $\tilde{\rho}^{(a)}$ and $\tilde{\rho}^{(s)}$ represent density perturbations associated with the acoustic wave and streaming motions, respectively. We require of our scaling that it: (i) be consistent with the tenets of the MADaM, (ii) correspond with the fundamental fast streaming scaling law Eq. (17) and associated velocity partition Eq. (28), and (iii) remain otherwise independent of any unsupported assumptions about the relative magnitudes of the terms. Defining the condensation $s = (\tilde{\rho} - \rho_0)/\rho_0$ and recalling a fundamental result of linear acoustics [53, 54],

$$M_a \approx \max |s|, \quad (40)$$

which holds for acoustic Mach numbers $M_a = U_a/c \ll 1$, we further define the $\mathcal{O}(1)$ condensation, $\bar{s} = s/M_a$, so that $s = M_a \bar{s}$. This motivates the density partition

$$\tilde{\rho} - \rho_0 = M_a \rho_0 \rho^{(a)} + M_s \rho_0 \rho^{(s)}, \quad (41)$$

where the streaming Mach number is defined such that $M_s = U_s/c$. The nondimensionalized density partition is then obtained as $\rho - 1 = M_a \rho^{(a)} + M_s \rho^{(s)}$. With $M_a/M_s = q_p S \sim 1$ —a restatement of the order of magnitude equivalence of the particle and streaming velocities—we have $\tilde{\rho}^{(s)} \sim \tilde{\rho}^{(a)}$.

The result is a clear departure from the classical analyses, where $\tilde{\rho}^{(s)} \ll \tilde{\rho}^{(a)}$ as a prerequisite for perturbation expansion. The result is similarly contrasted when compared with the assumption $\tilde{\rho}^{(s)} \gg \tilde{\rho}^{(a)}$ taken by Zaremba in developing his fast streaming framework [32, 55]. We note that Zaremba's density partition is based purely on this assumption and although of a similar mathematical form to his velocity partition, the components of the former have no direct physical association with the components in the latter. The partition Eq. (41) resolves these matters. As we will see further on, by using the partition described in Eq. (41) with the MADaM, one rigorously arrives at the (more typically assumed) incompressibility of the streaming field.

B. Nondimensionalization

The simplest approach to applying the MADaM is to first nondimensionalize the unpartitioned equations and then expand the operators and field variables in the result by using their respective nondimensional partitioned forms. The outcome of the first step in this process yields the nondimensionalized counterpart to Eq. (38),

$$\begin{aligned} & q_\lambda \bar{\rho} d_t D_t u_x - d_x(\bar{\rho} u_x) D_t u_x \\ & = q_\lambda^2 d_x^2(\bar{\rho} u_x) + 2 q_p q_\lambda^2 \theta d_x^2 d_t u_x + q_p^2 q_\lambda^2 d_t F_x, \end{aligned} \quad (42)$$

where we have set $\tilde{F}_x = \rho_0 U_a k F_x$. The nondimensional density has been reexpressed in terms of the quantity $\bar{\rho} = q_p + \frac{\varepsilon q_p}{q_\lambda} \rho^{(s)} + \frac{q_p^2}{q_\lambda} \rho^{(a)}$, with the authors' foreknowledge that this will simplify the partitioned analysis. Had we simply combined Eqs. (36) (*i.e.*, without the additional time differentiation step) and then nondimensionalized the result, we would have instead obtained

$$\bar{\rho} D_t u_x = -q_\lambda^2 d_x \bar{\rho}' + 2 q_\lambda^2 q_p \theta d_x^2 u_x + q_p^2 q_\lambda F_x, \quad (43)$$

where $\bar{\rho}' = \bar{\rho} - q_p$. We use both forms of the governing equation in the section that follows.

C. Partitioning

1. Damped acoustic wave

By substituting the partitioned field variables and differential operators into Eq. (42) and then expanding the result, one obtains a 162-term (*i.e.*, *finite-term*) expression that we write as

$$\mathcal{A} u_x^{(a)} = \partial_\tau F_x + \mathcal{O}(q_\lambda), \quad (44)$$

where we have defined the linear acoustic field operator $\mathcal{A} = \partial_\tau^2 - \partial_\xi^2 - 2\theta \partial_\tau \partial_\xi^2$. By discarding the higher order terms and setting the force equal to zero, we arrive at a first check on the consistency of the MADaM. Here

“acoustic field” describes the operator itself since its differential operations are applied entirely with respect to an acoustic spatiotemporal basis.

The leading order equation $\mathcal{A}u_x^{(a)} = 0$ is a pervasive result [29, 34, 46, 54] describing damped propagation of a linear acoustic wave within a dissipative medium. We take a similar position to Riley that, although the value of θ may be small—even comparably so with respect to q_λ —the $\mathcal{O}(2\theta)$ term must be included in order to account for attenuation. For an acoustic wave generated by the vibrating origin of a semiinfinite domain, the stationary solution to the damped wave equation is

$$\lim_{\tau \uparrow \tau_\infty} u_x^{(a)} \approx \exp[\iota(\kappa \xi - \tau)], \quad (45)$$

where $\kappa = \kappa_r + \iota \kappa_i$ with

$$\kappa_r = \sqrt{\frac{\sqrt{1 + 4\theta^2} + 1}{2(1 + 4\theta^2)}}, \quad (46a)$$

$$\kappa_i = \sqrt{\frac{\sqrt{1 + 4\theta^2} - 1}{2(1 + 4\theta^2)}}, \quad (46b)$$

and where $\kappa_i \approx \theta \ll 1$ and $\kappa_r \approx 1$ in water for frequencies relevant to this analysis. One will note that this is a substantially different result than that obtained by Riley [29, 56].

2. Transient Burgers streaming

We now return to Eq. (43) to extract the streaming equation. Substituting and expanding as in the previous section lead to a *finite* (though 47-term) expression, worth comparing to the infinite series produced by classical asymptotic expansions that is arbitrarily truncated for tractability. By setting the force term to zero and then applying the differential constraints, the expression is reduced to 34 terms, subdivided by order of magnitude, and distinguished by the MADaM scales. These are

$$\mathcal{O}(S^{-1}) = \mathcal{O}(q_p) \ll \mathcal{O}(q_\lambda) \ll 1, \quad (47)$$

where S^{-1} and q_p are sufficiently small in comparison to q_λ that we may take the successive approximation approach, expanding first in combinations of S^{-1} and q_p , and then subsequently in q_λ , while leveraging integral constraints as necessary. The leading order equation is equivalent to the acoustic field equation if the result of a separate MADaM continuity analysis is substituted. We avoid redundancy by omitting this analysis here.

We consider terms up to second order in combinations of S^{-1} and q_p . After applying the integral constraints, only five terms remain. In fact, applying our integral constraints to all terms that are first order in S^{-1} or q_p causes all such terms to vanish except for $S^{-1} q_\lambda^3 \partial_x \rho^{(s)}$ at $\mathcal{O}(q_\lambda^3)$ and $2S^{-1} q_\lambda^5 \theta \partial_x^2 u_x^{(s)}$ at $\mathcal{O}(q_\lambda^5)$. The latter of these will be dealt with momentarily. The former, expressed

as an ordinary equation, leads to our second consistency check. We have

$$\partial_x \rho^{(s)} \approx 0, \quad (48)$$

which, after solving and applying the homogenous source condition, leads to $\rho^{(s)}(x, t) \approx 0$. In other words, perturbations to the background density due to streaming flow are negligible and this flow may therefore be regarded as incompressible. This is a fundamental *result* of careful application of the MADaM. Traditionally, this is axiomatically assumed without rigorous justification.

Even further, applying the MADaM to mass conservation produces a third consistency check at leading order: $\rho^{(a)} = -\int_0^\tau \partial_\xi u_x^{(a)} d\tau'$. This agrees with results found elsewhere in the literature [1, 34]. When combined, these last two consistency checks validate, *a posteriori*, the nondimensionalization and partitioning defined in Eq. (41).

At second order in S^{-1} and/or q_p and first order in q_λ , we have

$$\langle u_x^{(a)} \partial_\xi u_x^{(a)} \rangle_{\xi, \tau} + \langle \rho^{(a)} \partial_\tau u_x^{(a)} \rangle_{\xi, \tau} = 0. \quad (49)$$

This represents an interesting departure from the standard analyses [31, 34], where one writes

$$\langle \partial_\xi \mathcal{L} \rangle_{\xi, \tau} = \langle \partial_\xi \mathcal{T} \rangle_{\xi, \tau} - \langle \partial_\xi \mathcal{U} \rangle_{\xi, \tau}, \quad (50)$$

in terms of the acoustic Lagrangian, $\mathcal{L} = \mathcal{T} - \mathcal{U}$, and where $\partial_\xi \mathcal{T} = u_x^{(a)} \partial_\xi u_x^{(a)}$ and $\partial_\xi \mathcal{U} = -\rho^{(a)} \partial_\tau u_x^{(a)}$ are the gradient of the kinetic and potential acoustic energies, respectively. By substituting the acoustic velocity for the acoustic density and utilizing Eq. (45), one finds that

$$\max_{\xi \geq \pi/\kappa_r} |\langle \partial_\xi \mathcal{L} \rangle_{\xi, \tau}| = \frac{\kappa_r}{2\pi} e^{-\frac{2\pi\kappa_i}{\kappa_r}} \sinh\left(\frac{2\pi\kappa_i}{\kappa_r}\right) \approx \kappa_i, \quad (51)$$

where the approximation is valid when $\kappa_r \approx 1$ and $\kappa_i \ll 1$. In fact, the exact expression satisfies Eq. (49) to good approximation up to the 40 GHz limit for which $Kn \sim 0.01$. Furthermore, it is evident that below 25 GHz, the vanishingly small value of the Lagrangian gradient average directly corresponds to the amount of attenuation over a single wave period: both are equal to κ_i . These details are apparent in Fig. 1.

Lastly, for combinations at second order in S^{-1} and q_p , and second order in q_λ , we obtain the streaming equation. We include in this equation our previously unused term $2S^{-1} q_\lambda^5 \theta \partial_x^2 u_x^{(s)}$, which encapsulates viscous dissipation in the streaming dynamics. Then the streaming flow is governed by the forced viscous Burgers equation

$$D_t u = \mu \partial_x^2 u + \eta_m^{-1} f_R(x), \quad (52)$$

where we have dropped the streaming superscript and x -coordinate directional subscript, and with the nondimensional viscosity, $\mu = q_\lambda/R$, written in terms of the streaming Reynolds number, $R = \rho_0 x_s U_s / \mu_l$. We have

defined the maximum (intra-system) streaming conversion efficiency,

$$\eta_m = (q_p S)^{-2}, \quad (53)$$

whose placement in Eq. (52) underscores the role of the Reynolds stress, $f_R = -\langle u^{(a)} \partial_x u^{(a)} \rangle_{\xi, \tau}$, as a transduction mechanism between the two fields. One notes the similarity between the factor $(q_p S)^2$ and the squared factor in Eq. (12) of Thomsen’s inverted pendulum example. The latter describes the restoring torque of the pendulum as a function of high-frequency forcing at small vibrational amplitudes. The nondimensional product $q \Omega$ carries an analogous meaning to $q_p S$ in the present analysis.

The fourth (and perhaps most important) consistency check is ascertained when comparing Eq. (52) with the result obtained by Rudenko and Soluyan [46] (p. 203, Eq. (3.28)). Using a reductive analysis of the incompressible axisymmetric Navier-Stokes equations, they have established a similar axial flow description. Included in the Rudenko and Soluyan result is an additional right-hand-side term that is proportional to $-g''(0)u$, where $g(r)$ is an assumed separable radial function having a finite second derivative along $r = 0$. The absence of such an expression in our analysis is expected given its origination in a one-dimensional domain. The remainder of our analysis is carried out excluding the additional term. Its exclusion is made possible by a commensurate reduction in forcing that is inherent in the one-dimensional system by not considering momentum entrainment near the source, which behaves as a McIntyre sink [31]. The accuracy of the simpler fast-streaming axial equation is verified in [see co-article].

The role of q_λ in divorcing the viscous term from the other streaming terms during the successive approach warrants discussion. This role is made clear in the definition of μ . The smallness of this term is representative of the steepness of the boundary layer gradient at the distal boundary. In our analysis, the characteristic distance over which the streaming maximum decays to the no-slip condition (*i.e.*, the viscous boundary layer thickness, $\delta_v = \sqrt{2\mu l / \rho_0 \omega}$) is much smaller than the wavelength. However, our statement $q_\lambda \ll 1$ in Eq. (47) is tantamount to “preconfiguring” the MADaM so that it returns “large scale” behaviors—that is, behaviors that characterize *bulk* streaming. Since the reverse is true for the viscous boundary layer ($\lambda / \delta_v \gg 1$), the analysis tends to exclude this term and consequently discards the boundary layer. This approximating behavior is inherited directly from the MDPM for rigid-body systems.

Inasmuch as it is instructive to do so, we initially proceed with the viscous term intact—that is, we set $q_\lambda = 1$, so that $\mu = R^{-1}$ —before removing it further along in the analysis in accordance with the original value, $q_\lambda \ll 1$.

Adapting f_R for use with Eq. (52) requires a change of variables from the small spatial scale of the acoustic forcing to the large spatial scale of the streaming flow

and leads to

$$D_t u = \mu \partial_x^2 u + \frac{\bar{\alpha}}{2\eta_m} \exp(-2\bar{\alpha}x), \quad (54)$$

where $\bar{\alpha} = \kappa_i / q_\lambda$ is the nondimensional, streaming-scale-adjusted attenuation coefficient. As written, Eq. (54) is given entirely in terms of “slow time” variable t and “large space” variable x , and can therefore be solved with the appropriate boundary conditions and resting initial conditions to obtain the full transient steaming field. Note that this is possible despite the fact that we have used spatiotemporal averaging operations to decouple the equations.

3. Steady Riccati streaming

In the absence of a general method for the analytical solution of nonlinear PDEs, the solution to the transient streaming Eq. (54) remains unknown to the authors and it must therefore be numerically solved. On the other hand, when analysing acoustofluidic systems, one’s goal is often the recovery of an equation for the *steady* streaming. In this aim we are fortunate, as the steady solution to Eq. (54) can be obtained in closed form for the most general viscous case, and therefore also for the particular inviscid case. After setting the unsteady term to zero, integrating over the spatial domain, and then rearranging the result, we have

$$\partial_x u + c_s u^2 \approx c_f (\exp(-2\bar{\alpha}x) - 1) + \partial_x u|_{x=0}, \quad (55)$$

where $c_s = -(2\mu)^{-1}$ and $c_f = -c_s / 2\eta_m$, and where the homogeneous condition at the origin has ensured that $u^2|_{x=0} = 0$. The result has the form of Riccati’s equation [57], for which a solution method exists that involves transforming Eq. (55) into a second order linear equation [58]. The result is

$$u_{\text{visc}} = \frac{\partial_x \phi}{c_s \phi}, \quad (56a)$$

$$\phi = I_\beta(h) + c_\phi I_{-\beta}(h), \quad (56b)$$

$$c_\phi = -\frac{I_{\beta+1}(h_0) + I_{\beta-1}(h_0)}{I_{-(\beta+1)}(h_0) + I_{-(\beta-1)}(h_0)}, \quad (56c)$$

$$h = h_0 \exp(-\bar{\alpha}x), \quad (56d)$$

where I denotes the modified Bessel function of the first kind, $\beta = h_0 \sqrt{(\partial_x u_x|_{x=0} - c_f) / c_f}$, and $h_0 = \sqrt{(c_s c_f) / \bar{\alpha}^2}$. Here $\partial_x u|_{x=0}$ is unique and corresponds to the value that causes the solution to satisfy the far boundary condition. Finding this value exactly is intractable due to its embedding in the Bessel function terms, so that a shooting type of iteration is necessary.

The steady, inviscid solution is obtained by inspection of Eq. (54): $u_{\text{invisc}} = \sqrt{\frac{1}{2\eta_m} (1 - \exp(-2\bar{\alpha}x))}$. Its dimensional form is

$$\tilde{u}_{\text{invisc}} = U_a \sqrt{\frac{1}{2} (1 - \exp(-2\alpha \tilde{x}))}, \quad (57)$$

where $\alpha = \kappa_i k$ is the “true” absorption coefficient. Mitome [59] obtained a similar result in his treatment of the Rudenko and Soluyan expression. We demonstrate the broader implications of Eq. (57) in the following section.

4. Near-source approximation

Expanding in a Taylor series, we write Eq. (57) as $\tilde{u}_{\text{invisc}} = U_a (\frac{1}{2} \sum_{n=1}^{\infty} \frac{(2\alpha\tilde{x})^n}{n!})^{1/2}$. If \tilde{x}_{ns} is a point sufficiently close to the source, then $2\alpha\tilde{x}_{ns} \ll 1$ and we have the approximation

$$\tilde{u}_{ns} = U_a \sqrt{\alpha\tilde{x}_{ns}}, \quad (58)$$

which describes the streaming profile within the vicinity of the source. Guided by an empirical assumption, Moudjed *et al.* [28] balance the nonlinear inertial terms with the acoustic forcing in order to derive a scaling relation similar to Eq. (58). The near-source condition is another point of departure from the classical theory. In Ref. [20], the slow streaming assumption is applied to the Eckart bulk streaming configuration, leading to the near-source condition $\tilde{u} \propto \alpha$. In Sec. IV (and in [see co-article]), we confirm that the square root dependence in Eq. (58) is appropriate for fast bulk streaming systems.

5. Limit on the streaming conversion efficiency

As noted earlier, within the 1D problem we have established, the inviscid solution represents a “bulk flow solution” that can be asymptotically matched to a corresponding boundary layer solution for ill-conditioned systems—systems which have, in a manner of speaking, “lost” a boundary condition. This implies Eq. (57) can be used to determine the maximum achievable streaming velocity for such a system. One obtains the maximum

$$\max_{\forall} \tilde{u} = U_a / \sqrt{2}, \quad (59)$$

alongside two modes for its realization: (i) at any fixed location, $x_s < \infty$, along a finite domain for arbitrarily large excitation frequency, $\tilde{u}_{\text{max}} = \lim_{f \uparrow \infty} \tilde{u}_{\text{invisc}}$, or (ii) “very far” from the source at fixed excitation frequency and with arbitrarily large domain length, $\tilde{u}_{\text{max}} = \lim_{x_s \uparrow \infty} \tilde{u}_{\text{invisc}}(x = x_s)$.

Dividing Eq. (59) through by U_a , squaring both sides, and referencing Eq. (53), one has that

$$\max_{\forall} \left(\frac{|\tilde{u}^{(s)}|}{U_a} \right)^2 = \max_{\forall} \eta_m = \frac{1}{2}, \quad (60)$$

so that the streaming law expressed by Eq. (59) may evidently be interpreted as an energetic limit on the streaming conversion efficiency of 50%. One notes that this limit is *entirely independent of the constitutive parameters*. The “for all” notation \forall has been used to distinguish

between the meaning of “maximum” used here and the meaning of maximum when used to describe, for example, the “maximum particle velocity.” In the latter case, we refer to the maximum with respect to a particular system configuration, whereas the former refers to the maximum “for all” possible system configurations described by this model.

Referring once more to Thomsen’s rigid-body inverted pendulum problem, we see that the analogy remains apt. The condition in Eq. (13) for a stiffness induced upright stable equilibrium position is equivalent to the requirement that the input-output efficiency be less than 50%.

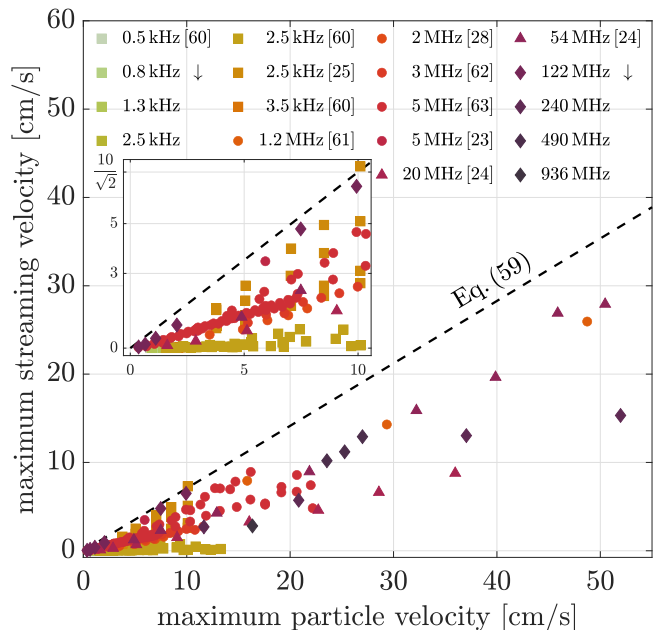


FIG. 2. Bulk streaming flows bounded by the maximum streaming law, Eq. (59). The data are taken from Refs. [23–25, 28, 60–63] (specified in legend) and represent eighteen data sets spanning eight separate studies. Data marker types are essentially log scale in frequency: (\square) $f < 1$ MHz, (\circ) $f \in [1, 10)$ MHz, (\triangle) $f \in [10, 100)$ MHz, and (\diamond) $f \in [100, 1000)$ MHz.

Before moving on we *strongly emphasize* that this streaming law is limited by its one dimensional construction. The most obvious consequence is that it is incapable of properly accounting for multi-dimensional effects, including advection of momentum flux away from the streaming axis (*i.e.*, beam widening), as well as generalized spatiotemporal resonance and anti-resonance due to reflection and refraction, and purposely defined spatial variations in the acoustic field, such as transducer focusing. Furthermore, we have assumed an isothermal system and while nonlinearity has been accounted for in the streaming field, it has been neglected in the acoustic field. Given the number and severity of these limitations, one might expect that Eq. (59) is likely little more than a mathematical curiosity. However, as we show further on,

this is not the case. A rather broad class of systems—that we refer to with the common nomenclature “bulk streaming”—evidently adhere to this limit.

IV. RESULTS

When solving the Burgers PDE Eq. (54), we employ the suite of components provided by the FEniCS Project [64–71]. When evaluating the viscous steady Riccati solution Eq. (56) in the most acutely ill-conditioned cases—where both computational efficiency and arbitrary precision operation are necessary—we have employed the Advanpix Multiprecision Computing MATLAB Toolbox [72].

A. Realization of maximum conversion efficiency

Assessment of the maximum achievable streaming law Eq. (59) is undertaken through comparison with experimental data reported in the literature. Studies were selected based on whether they adhere to the previously noted criteria—mainly, bulk acoustic streaming flows that are approximately laterally unbounded and that are driven by plane acoustic transducers. Studies were excluded if they did not fit this criteria or if they did not provide enough information for reliable estimation of both the on-source particle velocity and the maximum streaming velocity. Accordingly, the data were taken from eight separate studies [23–25, 28, 60–63] and encompass fifteen frequencies beginning in the audible spectrum and terminating well into the ultrasonic regime: 500 Hz to nearly 1 GHz. The survey results are shown in Fig. 2. The data from these studies evidently support the veracity of the streaming law. One set of data from Ref. [25] violates the law, though it does so in the mean value: the error bars from that study encompass the limit. Although boundary layer streaming has been excluded, it should be noted that data from such systems are expected to uniformly satisfy the law since they are typified by order of magnitude or larger separation between the on-source particle velocity and the maximum streaming velocity.

In the plots of Fig. 3, two special cases of the broader survey are presented. Both are taken from recent, rigorously undertaken and documented studies of Zhang *et al.* [25, 60]. The data involve bulk acoustic streaming generated by 2.5 kHz vibration of tip structures with radii of curvature (RoC) $\leq 5 \mu\text{m}$. Fig. 3(a) employs results from Ref. [60] to demonstrate the effect of varying viscosity with all else (including RoC) held constant. The results indicate that decreasing viscosity in these systems tends to increase the maximum streaming velocity, bringing the data closer to the law. This observation aligns with the inviscid approximation used in its derivation. In Fig. 3(b), we have plotted results from Zhang *et al.*’s earlier work [25] that characterize the effect of tip size, where

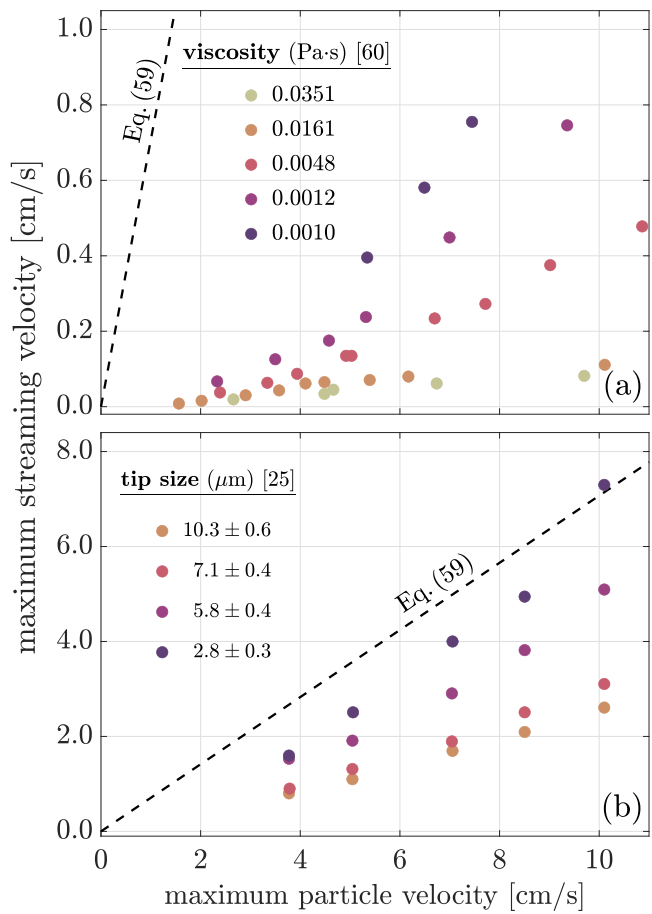


FIG. 3. Data representing studies done on bulk acoustic streaming generated by vibration of a sharp tip structure at 2.5 kHz [25, 60]. These are special cases of the broader survey shown in Fig. 2. In subplot (a), the inverse relationship between viscosity and maximum streaming velocity aligns with the inviscid assumption used in the derivation of the streaming law. In subplot (b), tip size is twice the radius of tip curvature. As tip size is decreased, the magnitude and trend of the data approach the streaming law. This suggests that the one-dimensional model is congruent with an upper bound defined by a “one-dimensional tip.”

they define tip size as 2RoC . The data show that as tip size is decreased, the profile approaches the streaming law, both in terms of magnitude and in terms of trend. This suggests congruence of the one-dimensional model with a physical “one-dimensional tip” system. The single data point that weakly violates the streaming law is the same that was previously noted.

B. Shared physics of bulk streaming systems

Eckart streaming is the net bulk flow generated by an acoustic source within a bounded fluid medium when the far boundary is a perfect acoustic absorber (Fig. 4(a)).

Equation (52) assigns physical provenance to the transient layering behavior that is empirically observed in such systems. The viscous flow solution Eqs. (56) defines the “shark fin” (*i.e.*, rounded sawtooth) profile that is characteristic of steady axial Eckart flow [23]. The Burgers-Riccati physics of fast axial Eckart flow is closely attended to in [see co-article]. In the limit of the inviscid approximation, the Eckart system “loses” a boundary condition and the result can be interpreted as the bulk flow solution, absent a very thin boundary layer. We will show how this inviscid solution is related to Stuart-Lighthill “jet” streaming.

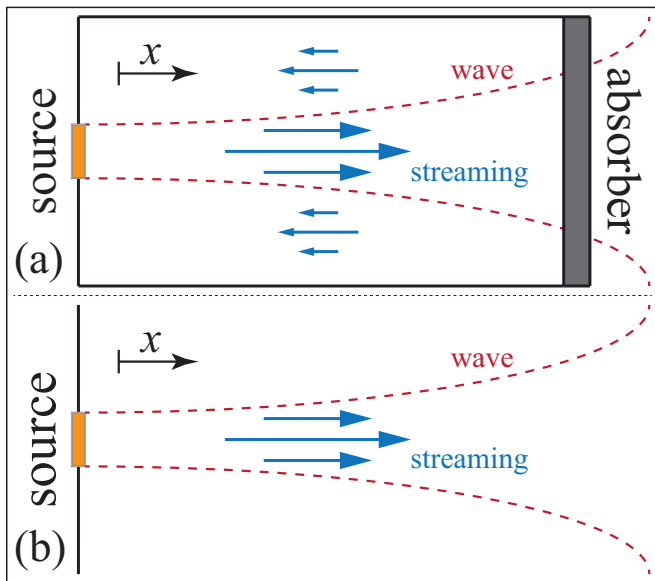


FIG. 4. Simplified diagram depicting bulk acoustic streaming types. (a) Eckart streaming and (b) Stuart-Lighthill “jet” streaming. In either scenario, the near-source behavior is that of a McIntyre sink [31]. In (a), the continuation of the acoustic wave beyond the boundary is representative of the fact that one can replace the perfect absorber with an acoustically transparent membrane (*e.g.*, Saran Wrap) to achieve a similar effect, as illustrated in Ref. [20].

Lighthill’s seminal acoustic streaming study [31] is one of the most well known and oft-cited works on the topic. It addresses, among other subjects, the description of bulk turbulent jet streaming within an unbounded medium (Fig. 4(b)). The jet streaming is generated from high-frequency (≥ 1 MHz) acoustic forcing that Lighthill treated as a point source in light of the relatively large associated attenuation coefficient. In the modern applied acoustofluidics setting, flow dynamics within the attenuation length scales of such high-frequency acoustics are important and the source must be treated more carefully. The point-source treatment invokes a singularity as $x \downarrow 0$ that has no observable physical analog. Experiment reveals zero velocity at the source with near-source algebraic growth mediated in the far field by long-tailed decay, this mediation leading to a well-defined maximum.

In a recent study, Dentry *et al.* [24] attempted to rectify these issues by modifying Lighthill’s model to account for a finite source area and for laminar streaming. Laminarity is evident in viscous liquids by direct observation. While the study provides useful insights toward achieving its broader objectives, it is hindered by a number of errors that stem from two important oversights: (i) an incorrectly stated equation that was later discussed (though never completely addressed) in a published erratum [52], and (ii) the determination of streaming flow with particle image velocimetry (PIV) by utilizing $a \approx 5 \mu\text{m}$ diameter particles with very high frequency (small wavelength) acoustic sources. Errors associated with item (i) require a factor of ≈ 2.65 correction when made directly to the acoustic power. They affect model accuracy and whether the data is correctly represented in the study. Error source (ii) is important because for $a \gtrsim \lambda$, effects of the acoustic radiation force on the particle become significant and the particle does not reliably follow the streaming field. This invalidates data for $f \geq 240$ MHz which equates to a third of the experimental data in Ref. [24].

The Lighthill and Dentry models for bulk jet streaming into an unbounded medium admit a general form

$$\tilde{u}_d(\tilde{r}, \tilde{x}) = \sqrt{\frac{2P}{\pi \rho c S(\tilde{x})^2}} \sqrt{1 - \exp(-2\alpha \tilde{x})} \times \exp\left[-\left(\frac{\tilde{r}}{S(\tilde{x})}\right)^2\right], \quad (61)$$

where \tilde{r} denotes the radial coordinate and for simplicity we have assumed an ideal (*i.e.*, uniform acoustic intensity) circular thickness-mode transducer. The length S is obtained as the numerical solution to a stiff ODE. It accounts for the spatial rate of lateral losses by normalizing a transverse Gaussian decay. The length S also enforces far field axial velocity decay via multiplicative attenuation.

If we “eliminate” the lateral dimensionality by considering only the jet axis ($\tilde{r} = 0$) and fixing $S = 2\sqrt{A/\pi}$, then the jet-streaming model of Eq. (61) simplifies identically to the inviscid Riccati solution of Eq. (57). In fact, Lighthill’s semi-empirical derivation initially produces a one-dimensional model of exactly this form. He subsequently extends the model to include lateral dimensionality by assuming Gaussian decay of the streaming velocity away from the jet axis. The fundamental difference in our approach is that we have derived Eq. (57) directly from the Navier-Stokes equations. Its form originates in the nonlinear terms of Eq. (52), and these are regarded as dominant in the MADaM analysis as a direct consequence of the large-amplitude streaming assumption.

We avoid the computational demand of Lighthill’s approach by obtaining a highly-simplified algebraic closed-form model for the axial streaming profile directly from the steady-state Riccati physics. We achieve this by first deriving a scaling relation between the power and the

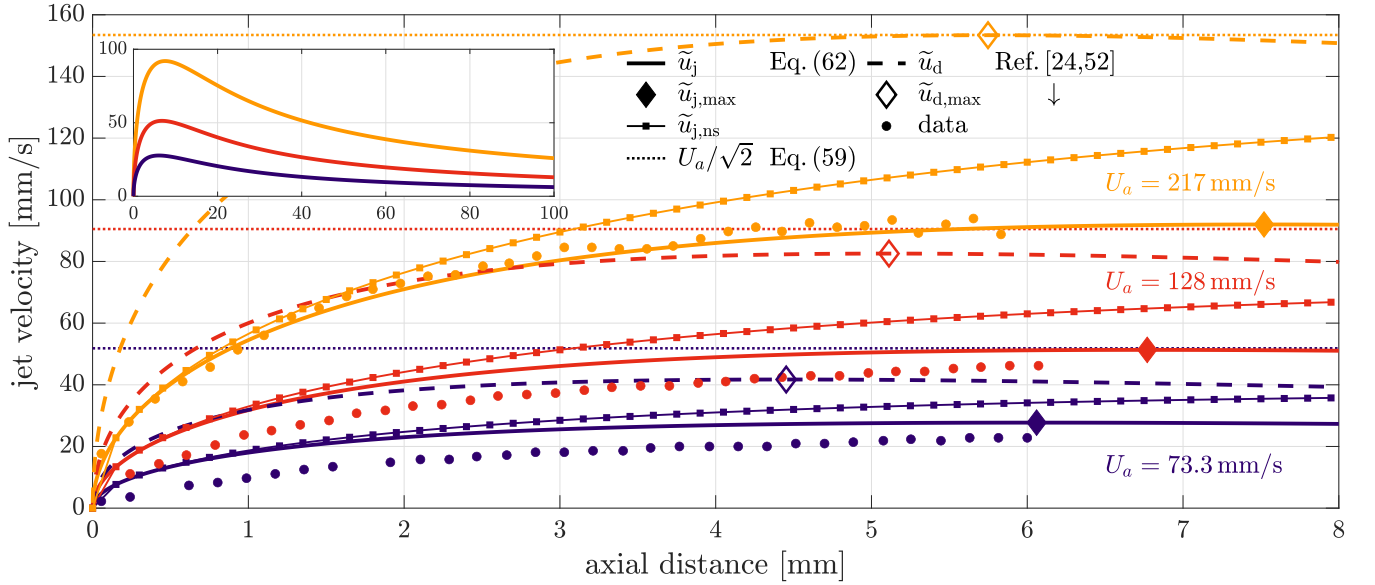


FIG. 5. Stuart-Lighthill jet streaming axial profiles at three different acoustic forcing magnitudes. Data and reference (laminar) models are taken from Ref. [24] with corrections applied according to the erratum in Ref. [52]. The attenuation prefactor used with \tilde{u}_j is derived to satisfy two boundary conditions. Near the source, the profile agrees asymptotically with Eq. (58). Away from the source, the profile maximum is enforced to occur at x_s , where x_s is estimated from the Buckingham II scaling relation of Eq. (64). Thus, the curvature, maximum amplitude, and location of the maximum are systematically enforced from Eq. (57). A high-level perspective of the efficacy of this approach is provided in Fig. 6.

axial location of the streaming maximum (with Buckingham's II theorem). This is used in conjunction with an attenuation prefactor and boundary conditions to account for advection of momentum away from the jet axis. The details are included in [cite supplemental materials]. The analysis is carried out with the valid PIV regime data ($f \leq 122$ MHz) from Ref. [24]. Where necessary, the data and models from that study are corrected according to the associated erratum [52]. The result of these efforts is the inviscid model of Eq. (57) modified by the attenuation prefactor:

$$\tilde{u}_j = B(\tilde{x}) \tilde{u}_{\text{invisc}}, \quad (62)$$

where

$$B(\tilde{x}) = \frac{1 - \exp(2\alpha x_s) + \alpha x_s}{1 - \exp(2\alpha x_s) + \alpha(x_s - \tilde{x})}, \quad (63)$$

and

$$x_s = \frac{34 P^{0.1}}{\rho_0^{0.1} \alpha^{0.5} f^{0.3}}, \quad (64)$$

is the Buckingham-II estimate of the axial distance to maximum streaming velocity. The accuracy of Eq. (64) is illustrated in [supplementary materials, Fig. 2]. The boundary conditions are chosen so that \tilde{u}_j attains its maximum at x_s and the near-source inertia-dominant regime is asymptotically equivalent to Eq. (58). In other words, the model is primarily established by the steady Riccati physics.

The leading portion of the axial jet profile is examined in Fig. 5. This portion of the flow is a mechanistic analog for steady Eckart streaming through Eq. (57). The models and data are shown for fixed frequency at three different source velocities. The near-source jet velocity, $\tilde{u}_{j,ns} = B(x) \tilde{u}_{ns}$, is also shown. Aside from the obvious improvement in amplitude correspondence, Eq. (62) enforces a downstream shift in the maximum streaming velocity distance estimate. Since the data are monotonic with an apparently nonzero slope, the shift represents an increase in accuracy. Within the vicinity of the source, the profile curvature is evidently better explained by the closed-form model. This region is strongly correlated to the near-source approximation, which itself originates in the inviscid Riccati solution. At smaller amplitudes, the valid range of the near-source approximation extends roughly to x_s .

The streaming maxima for the data and models are plotted as a continuous function of maximum particle velocity in Fig. 6. Overall, the closed-form model provides the most faithful characterization of the observations. It does so at a significant reduction in computational cost, since the other models involve the numerical integration of stiff, nonlinear ODEs. The physical constraints of the closed-form model ensure its adherence to the streaming law. The Dentry model and modified Lighthill model both violate the law. The systematically low-valued data in Fig. 5(d) are an inaccurate accounting of the streaming flow due to the effects of acoustic radiation forcing on the $5 \mu\text{m}$ PIV particles.

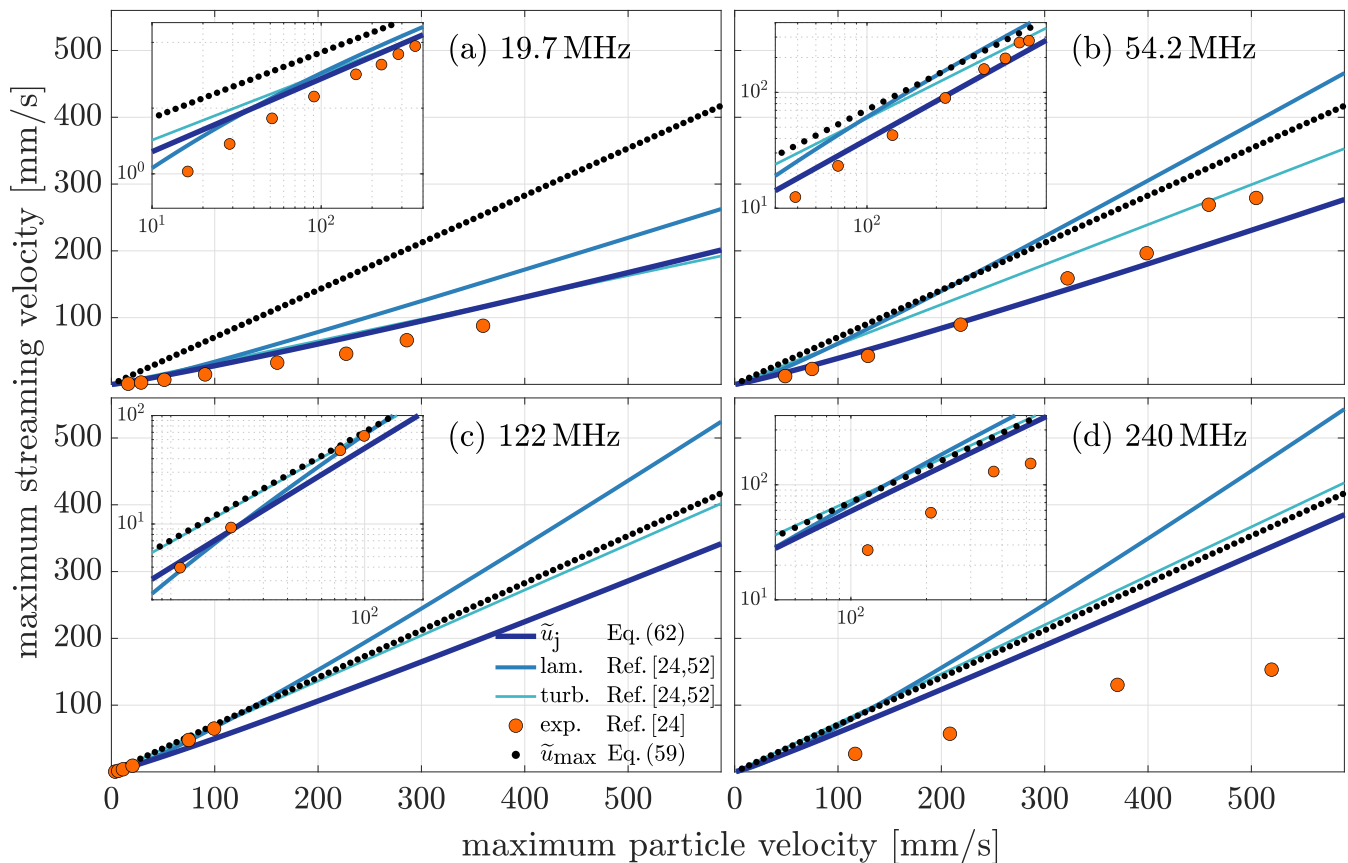


FIG. 6. Maximum velocity profiles for steady Stuart-Lighthill jet streaming at differing acoustic forcing frequencies. Overall, Eq. (62)—with attenuation properties enforced to satisfy Eqs. (58) and Eq. (64)—better accounts for the observed behaviors. Its algebraic form ensures computational efficiency. The streaming law is evidently violated by the Lighthill and Dentry models, while Eq. (62) adheres to the law by construction. The systematically low-valued data from Ref. [24] in subplot (d) is likely spurious as a result of significant acoustic radiation forcing. This is due to the relatively small acoustic wavelength— $\lambda \lesssim 6 \mu\text{m}$ for $f \gtrsim 240 \text{ MHz}$ —compared to the PIV particle size, $5 \mu\text{m}$.

The closed form model is used in conjunction with an inviscid Burgers equation (*i.e.*, Eq. (52) with μ set to zero) to approximate the transient flow development of the Stuart-Lighthill jet. We consider the leading profile of the jet, from the source to the axial coordinate of the velocity maximum. The transient component of the streaming field is extracted with the nondimensional transient energy density:

$$\langle \mathcal{E}_{\delta u} \rangle_x(t) = \frac{1}{2} \int_0^1 \delta u(x,t)^2 dx, \quad (65)$$

where the nondimensional background density is unity, $dV = dx$, and $\delta u(x,t) = u(x,t) - u(x,t-dt)$ is the transience of the Burgers streaming field. The transient flow behaviors are brought to light in Fig. 7. The most striking features develop about the nonmonotonicity of time to steadiness as a function of acoustic frequency. They suggest high frequency trend reversals. In the plots, we have implicitly defined steadiness as $\langle \mathcal{E}_{\delta u} \rangle_x < 10^{-9}$. In Fig. 6(a), two trend reversals are observed, a minor re-

versal at $\sim 100 \text{ MHz}$ and a major reversal at $\sim 256 \text{ MHz}$. Above the latter, time to steadiness appears to be an increasing function of frequency, despite a fixed on-source particle velocity and decreasing vibrational amplitude. A corresponding trend reversal is observed in the frequency isolines of the inset surface plot. The isolines correspond to the profiles plotted in Fig. 6(b) and reveal three regimes. At frequencies below the minor reversal, transient energy is more evenly distributed and exhibits smooth rolloff into steadiness. As frequency is increased to within the minor reversal, transient decay is linear in log-log space (*i.e.*, follows a power law, see 64 MHz and 128 MHz). This culminates in the formation of an energy peak near the terminal profile edge for frequencies approaching the major reversal. With peak formation, decay to steadiness evolves from “smooth and slow” toward “sharp and instantaneous.” Above $\sim 256 \text{ MHz}$, the energy peak shifts away from the steady edge, leading to the development of a local maximum.

We now consider the effect of the frequency on the

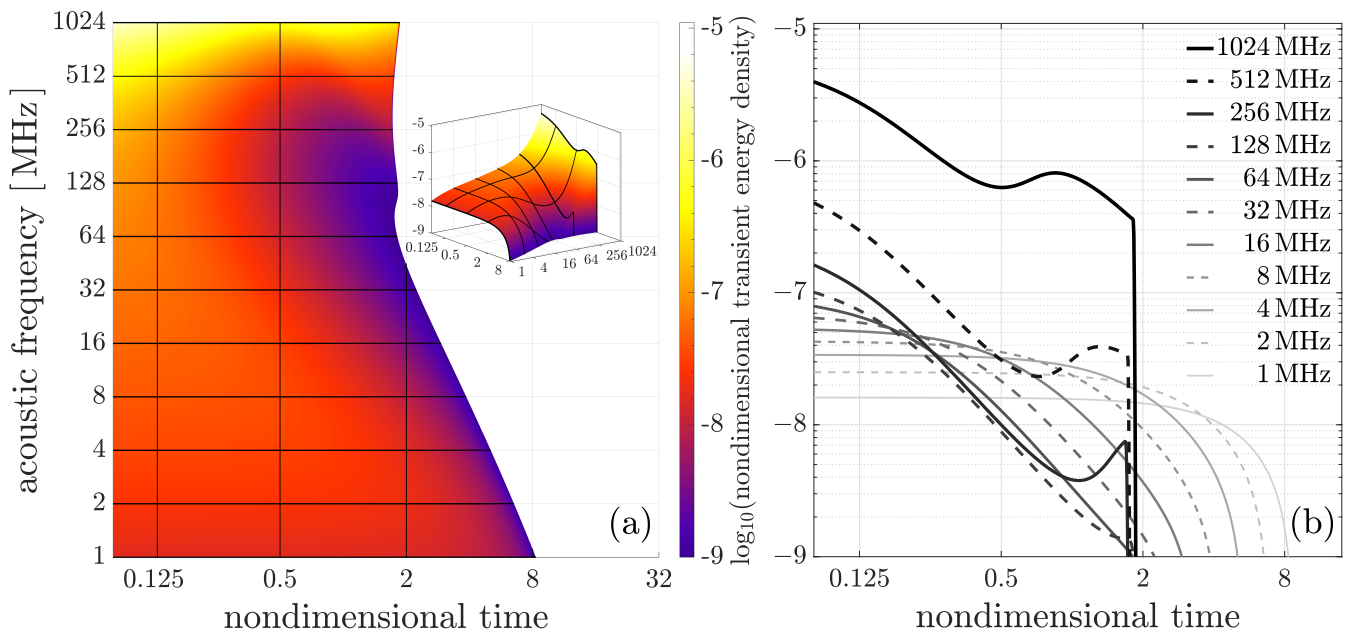


FIG. 7. Transient energy density for the leading portion of the Stuart-Lighthill jet profile. The transient dynamics are extracted from the net streaming flow with definition Eq. (65). In subplot (a), time to steadiness is a non-monotonic function of frequency exhibiting trend reversals at ~ 100 MHz and ~ 256 MHz. Frequency isolines in the surface inset correspond to solid profiles in plot (b), where three regimes are observed. At low frequencies, evenly distributed transient energy rolls off quickly into steadiness. At moderate frequencies, power-law transient decay gives way to energy peak development at the terminal end and instantaneous decay to steadiness. At high frequencies, the peak shifts away from the terminal edge and defines a local maximum.

steady streaming profile in Fig. 8 through the use of the closed-form model while maintaining a constant acoustic intensity (and power) from the source. With the assumption of uniform intensity over the emitting surface, we have $U_a = 2\pi f \xi_p = \sqrt{\frac{I}{z_0}} = \sqrt{\frac{P/A}{z_0}}$ for a device of fixed area A and with $z_0 = \rho_0 c$ as the acoustic impedance of the fluid. The profiles in the plot demonstrate that the theoretical maximum is achieved over a shorter distance as frequency is increased and power is held constant. Over a majority of the domain, the streaming velocity is approximately linearly incremented in response to a logarithmically incremented frequency grid. Since the streaming law Eq. (59) is non-constitutive, the observed relationship implies that for inviscid systems where approximation Eq. (57) is valid, the only means for attaining the theoretical maximum streaming velocity within a fixed domain is by increasing the acoustic frequency. Though the maximum streaming velocity is directly proportional to the vibrational amplitude, the exponential factor representing the Reynolds stresses attains its maximum value as the square root of a Gaussian function of increasing frequency ($\alpha \propto \omega^2$) and is independent of vibrational amplitude.

V. CONCLUDING REMARKS

Over the last several decades, advancements in the area of acoustofluidics have brought within practical reach a bevy of useful applications servicing an expansive disciplinary scope. This rapid innovation has left myriad physical curiosities orphaned from cogent description scattered in its wake. This deficit unsurprisingly originates in the intractable governing nonlinear equations of motion. Classical efforts to systematically surmount this difficulty were initiated by Lord Rayleigh in his pivotal investigations of acoustic streaming nearly one hundred fifty years ago.

Rayleigh's methods provided the template for a procession of similar techniques over the course of the subsequent century by notable acousticians and fluid mechanicians. The common vein throughout is a temporal decomposition of the fluid motion into an acoustic field and a steady flow field that is either wholly or partially driven by acoustic streaming. In the more than forty years since Lighthill exposed how such assertions cannot be extended to the frequencies and amplitudes routinely in use, since only modest headway has been made toward a more comprehensive approach.

This study has detailed an apt modernization of the traditional perturbative technique. Our framework, the Multiscale Articulated Differentials Method, has flexi-

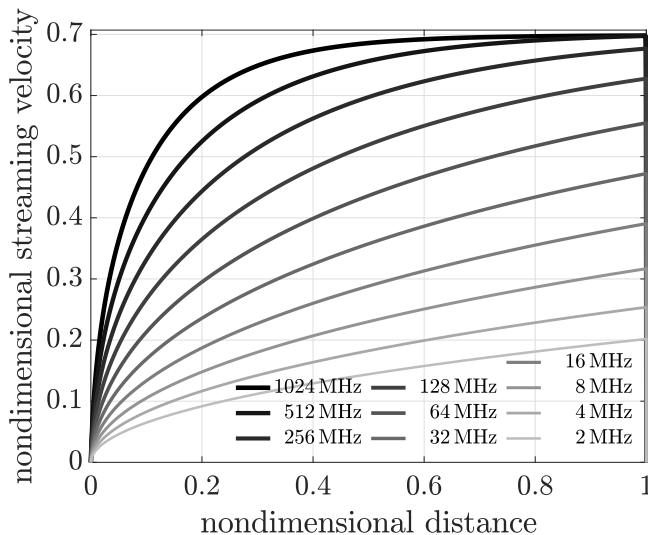


FIG. 8. Steady streaming velocity profiles for a logarithmic frequency space defined over a fixed acoustic intensity (and power). Only the highest frequency attains the theoretical maximum streaming velocity in the finite domain. Though the maximum streaming velocity is itself directly proportional to the maximum vibration amplitude, the evolution of the jet velocity over the distance from the acoustic source depends on the Reynolds stress, as shown in Eq. (57). The Reynolds stress term attains its maximum as the square root of a Gaussian function of increasing frequency, since $\alpha \propto \omega^2$.

bility and generality as its underpinnings. The method adopts the unconventional means of differentiating across

the vast spatiotemporal scale disparities typical in high-frequency acoustofluidics. The key result of this undertaking is a field-decoupled, finite-term expansion of the governing equations, with terms stratified by order of importance and catalyzed by the disparities themselves.

We investigated the efficacy of the method by applying it to a simple one-dimensional problem under the large-amplitude streaming assumption. The nonlinear equations of motion approximating the fast axial streaming were recovered and it was shown that, for the one-dimensional problem, the transient system is written as a viscous Burgers equation forced by the Reynolds stresses of the acoustic wave. The Burgers description reduces, at steady state, to a Riccati equation. We have thoroughly characterized the Burgers-Riccati system as it relates to Eckart streaming, Stuart-Lighthill streaming, and other recently studied forms of bulk acoustic streaming. Using an inviscid approximation, we derived simple expressions for the near-source inertial streaming behavior and the maximum attainable streaming velocity. From the latter, we recovered a universal upper bound on the streaming conversion efficiency of 50%. These findings were rigorously validated by comparison to theoretical and experimental findings from a broad survey of the literature.

ACKNOWLEDGMENTS

The work presented here was generously supported by a SERF research grant to J. Friend from the W. M. Keck Foundation. He is furthermore grateful for the support of this work by the Office of Naval Research (Grant No. 12368098). J. Orosco is thankful for support provided by the University of California's Presidential Postdoctoral Fellowship Program.

-
- [1] J. Friend and L. Y. Yeo, *Rev. Mod. Phys.* **83**, 647 (2011).
 - [2] A. Bussonnière, A. Antkowiak, F. Ollivier, M. Baudoin, and R. Wunenburger, *Phys. Rev. Lett.* **124**, 084502 (2020).
 - [3] B. Orazbayev and R. Fleury, *Phys. Rev. X* **10**, 031029 (2020).
 - [4] S. Karthick and A. K. Sen, *Phys. Rev. Applied* **10**, 034037 (2018).
 - [5] N. Zhang, J. P. Zuniga-Hertz, E. Y. Zhang, T. Gopesh, M. J. Fannon, J. Wang, Y. Wen, H. H. Patel, and J. Friend, *Lab Chip* (2021).
 - [6] W. Connacher, J. Orosco, and J. Friend, *Phys. Rev. Lett.* **125**, 184504 (2020).
 - [7] T. Gibaud, N. Dagès, P. Lidon, G. Jung, L. C. Houré, M. Sztucki, A. Poulesquen, N. Hengl, F. Pignon, and S. Manneville, *Phys. Rev. X* **10**, 011028 (2020).
 - [8] J. N. Belling, L. K. Heidenreich, Z. Tian, A. M. Mendoza, T.-T. Chiou, Y. Gong, N. Y. Chen, T. D. Young, N. Wattanatorn, J. H. Park, L. Scarabelli, N. Chiang, J. Takahashi, S. G. Young, A. Z. Stieg, S. D. Oliveira, T. J. Huang, P. S. Weiss, and S. J. Jonas, *PNAS* **117**, 10976 (2020).
 - [9] A. Huang, H. Liu, O. Manor, P. Liu, and J. Friend, *Adv. Mater.* **32**, 1907516 (2020).
 - [10] G. Lajoinie, T. Segers, and M. Versluis, *Phys. Rev. Lett.* **126**, 034501 (2021).
 - [11] C. J. Benmore and J. K. R. Weber, *Phys. Rev. X* **1**, 011004 (2011).
 - [12] J. Blamey, L. Y. Yeo, and J. R. Friend, *Langmuir* **29**, 3835 (2013).
 - [13] X. Xu, Q. Wu, H. Chen, H. Nassar, Y. Chen, A. Norris, M. R. Haberman, and G. Huang, *Phys. Rev. Lett.* **125**, 253901 (2020).
 - [14] M. Plaksin, S. Shoham, and E. Kimmel, *Phys. Rev. X* **4**, 011004 (2014).
 - [15] Z. Yang, F. Gao, X. Shi, X. Lin, Z. Gao, Y. Chong, and B. Zhang, *Phys. Rev. Lett.* **114**, 114301 (2015).
 - [16] W. Connacher, N. Zhang, A. Huang, J. Mei, S. Zhang, T. Gopesh, and J. Friend, *Lab Chip* **18**, 1952 (2018).
 - [17] J. S. Bach and H. Bruus, *Phys. Rev. Lett.* **124**, 214501 (2020).
 - [18] J. W. Strutt, *Philos. T. Roy. Soc. Lon.* **175**, 1 (1884).
 - [19] C. Eckart, *Phys. Rev.* **73**, 68 (1948).
 - [20] W. L. M. Nyborg, in *Physical Acoustics*, Properties of Polymers and Nonlinear Acoustics, Vol. 2, edited by W. P. Mason (Academic Press, New York, 1965) pp. 265–

- 331.
- [21] P. J. Westervelt, *J. Acoust. Soc. Am.* **25**, 60 (1953).
- [22] I. Reynt, H. Bailliet, and J.-C. Valière, *J. Acoust. Soc. Am.* **135**, 27 (2014).
- [23] T. Kamakura, T. Sudo, K. Matsuda, and Y. Kumamoto, *J. Acoust. Soc. Am.* **100**, 132 (1996).
- [24] M. B. Dentry, L. Y. Yeo, and J. R. Friend, *Phys. Rev. E* **89**, 013203 (2014).
- [25] C. Zhang, X. Guo, P. Brunet, M. Costalonga, and L. Royon, *Microfluid Nanofluid* **23**, 104 (2019).
- [26] V. Daru, I. Reynt, H. Bailliet, C. Weisman, and D. Baltean-Carlès, *J. Acoust. Soc. Am.* **141**, 563 (2017).
- [27] G. P. Chini, Z. Malecha, and T. D. Dreeben, *J. Fluid Mech.* **744**, 329 (2014).
- [28] B. Moudjed, V. Botton, D. Henry, H. Ben Hadid, and J.-P. Garandet, *Phys. Fluids* **26**, 093602 (2014).
- [29] N. Riley, *Annu. Rev. Fluid Mech.* **33**, 43 (2001).
- [30] J. Vanneste and O. Bühler, *P. Roy. Soc. A-Math. Phys.* **467**, 1779 (2011).
- [31] J. Lighthill, *J. Sound Vib.* **61**, 391 (1978).
- [32] L. K. Zarembo, in *High-Intensity Ultrasonic Fields*, edited by L. Rozenberg (Springer, New York, 1971).
- [33] H. Bailliet, V. Gusev, R. Raspet, and R. A. Hiller, *J. Acoust. Soc. Am.* **110**, 1808 (2001).
- [34] A. Riaud, M. Baudoin, O. Bou Matar, J.-L. Thomas, and P. Brunet, *J. Fluid Mech.* **821**, 384 (2017).
- [35] This can be readily observed by comparing Eqs.(2.4), (2.7), and (4.15) in the referenced study. The length scale in question characterizes the interior flow. In practice, this length can be quite large.
- [36] Calculation performed in meeting with John Thomas, Ph.D., President and Founder of M-Star CFD, a lattice Boltzmann-based simulation framework (2020).
- [37] C. McIntyre, A. M. Yao, G. L. Oppo, F. Prati, and G. Tissoni, *Phys. Rev. A* **81**, 013838 (2010).
- [38] G.-L. Oppo, A. M. Yao, F. Prati, and G. J. de Valcárcel, *Phys. Rev. A* **79**, 033824 (2009).
- [39] I. Battiato and D. M. Tartakovsky, *J. Contam. Hydrol. Reactive Transport in the Subsurface: Mixing, Spreading and Reaction in Heterogeneous Media*, **120-121**, 18 (2011).
- [40] T. D. Scheibe, E. M. Murphy, X. Chen, A. K. Rice, K. C. Carroll, B. J. Palmer, A. M. Tartakovsky, I. Battiato, and B. D. Wood, *Groundwater* **53**, 38 (2015).
- [41] L. A. Magrini, M. O. Domingues, E. E. N. Macau, and I. Z. Kiss, *Chaos* **30**, 063139 (2020).
- [42] D. Aubry and G. Puel, *IOP Conf. Ser.: Mater. Sci. Eng.* **10**, 012113 (2010).
- [43] A. A. Robel, G. H. Roe, and M. Haseloff, *J. Geophys. Res.-Earth* **123**, 2205 (2018).
- [44] B. Pottier, A. Raudsepp, C. Frétygny, F. Lequeux, J.-F. Palierne, and L. Talini, *J. Rheol.* **57**, 441 (2013).
- [45] M. E. Cates, *Macromolecules* **20**, 2289 (1987).
- [46] O. V. Rudenko and S. I. Soluyan, *Theoretical Foundations of Nonlinear Acoustics*, Studies in Soviet Science (Plenum, New York, 1977).
- [47] I. I. Blekhman, *Vibrational Mechanics: Nonlinear Dynamic Effects, General Approach, Applications* (World Scientific, River Edge, NJ, 2000).
- [48] J. J. Thomsen, *Vibrations and Stability: Advanced Theory, Analysis, and Tools*, 2nd ed. (Springer-Verlag, Berlin Heidelberg, 2003).
- [49] J. J. Thomsen, *J. Sound Vib.* **253**, 807 (2002).
- [50] B. Moudjed, V. Botton, D. Henry, S. Millet, J.-P. Garandet, and H. Ben-Hadid, *Appl. Phys. Lett.* **105**, 184102 (2014).
- [51] C.-G. Yao, Z.-W. He, and M. Zhan, *Chinese Phys. B* **22**, 030503 (2013).
- [52] M. B. Dentry, L. Y. Yeo, and J. R. Friend, *Phys. Rev. E* **94**, 059901 (2016).
- [53] R. T. Beyer, *Nonlinear Acoustics* (American Inst. of Physics, 1997).
- [54] V. A. Shutilov, *Fundamental Physics of Ultrasound* (Gordan and Breach Science Publishers, New York, NY, 1988).
- [55] This is partially due to the fact that in the referenced study, the streaming field variable definitions ambiguously encompass the unperturbed “background” field variables.
- [56] In the referenced study, one readily verifies that the solution given in Eq.(9) does not satisfy the first-order damped equation obtained from Eq. (8).
- [57] J. Riccati, *Acta Erud.* **8**, 66 (1724).
- [58] E. Ince, *Ordinary Differential Equations* (Dover, New York, 1956).
- [59] H. Mitome, T. Kozuka, and T. Tuziuti, *Jpn. J. Appl. Phys.* **34**, 2584 (1995).
- [60] C. Zhang, X. Guo, L. Royon, and P. Brunet, *Micromachines* **11**, 607 (2020).
- [61] S. N. Makarov, N. G. Semenova, and V. E. Smirnov, *Fluid Dyn.* **24**, 823 (1989).
- [62] V. Frenkel, R. Gurka, A. Liberzon, U. Shavit, and E. Kimmel, *Ultrasonics* **39**, 153 (2001).
- [63] H. Mitome, *Electr. Commun. Jpn.* **81**, 1 (1998).
- [64] M. S. Alnæs, A. Logg, K.-A. Mardal, O. Skavhaug, and H. P. Langtangen, *Int. J. Comput. Sci. Eng.* **4**, 231 (2009).
- [65] M. S. Alnæs, J. Blechta, J. Hake, A. Johansson, B. Kehlet, A. Logg, C. Richardson, J. Ring, M. E. Rognes, and G. N. Wells, *Arch. Num. Sofwr.* **3**, 9 (2015).
- [66] M. S. Alnæs, A. Logg, K. B. Ølgaard, M. E. Rognes, and G. N. Wells, *ACM Trans. Math. Softw.* **40**, 9:1 (2014).
- [67] R. C. Kirby, *ACM Trans. Math. Softw.* **30**, 502 (2004).
- [68] R. C. Kirby and A. Logg, *ACM Trans. Math. Softw.* **32**, 417 (2006).
- [69] A. Logg, K.-A. Mardal, and G. N. Wells, eds., *Automated Solution of Differential Equations by the Finite Element Method: The FEniCS Book*, Lecture Notes in Computational Science and Engineering (Springer-Verlag, Berlin Heidelberg, 2012).
- [70] A. Logg and G. N. Wells, *ACM Trans. Math. Softw.* **37**, 20:1 (2010).
- [71] K. B. Ølgaard and G. N. Wells, *ACM Trans. Math. Softw.* **37**, 8:1 (2010).
- [72] P. Holoborodko, *Multiprecision Computing Toolbox for MATLAB*, Advanpix LLC (2020).